Magnetized Taub adiabat and the *PT* characteristics of magnetic neutron stars

Ritam Mallick* and Shailendra Singh
Indian Institute of Science Education and Research Bhopal, Bhopal, India

(Received 16 August 2018; revised manuscript received 3 June 2019; published 10 July 2019)

In this study, we derive the magnetized Taub adiabat (TA) equation from the hydrodynamic conservation conditions. For the conversion of one phase to other the combustion adiabat (CA) equation is the same as the TA equation, only the equation of state (EoS) of the upstream phase is different from that of the EoS of the downstream phase. We employ the magnetized CA equations to study the evolution of a magnetized neutron star to a magnetized quark star. The pressure of the burnt quark matter has a maximum, which indicates a bound on the maximum mass of the quark star. The central density of the neutron star and the angle between the rotation axis and the magnetic axis (defined as the tilt angle) are seen to be significant in determining the magnetic field, and the tilt of the quark star. The magnetic field and the tilt of the quark star can have important observational significance and can help in understanding the physics at high density and strong magnetic field.

DOI: 10.1103/PhysRevC.100.015801

I. INTRODUCTION

Shock fronts are generally depicted by a discontinuous change in the characteristics of the medium propagating faster than the speed of sound in that medium. In most plasmas, the width of the shock front is very thin, and it is usually considered to be a one-dimensional plane of discontinuity [1]. Taub [2] was the first to study the relativistic hydrodynamic shocks. He used the mass, momentum, and energy conservation laws to derive the relativistic Rankine-Hugoniot (RH) conditions. De Hoffmann and Teller [3] first performed the theoretical treatment of hydrodynamic shocks in the presence of a magnetic field, which was immediately followed by an avalanche of theoretical studies [1,4]. However, the relativistic treatment of magnetized hydrodynamic shocks was first done by Lichnerowicz [5,6]. Other important works in this field were successively carried out by Appl and Camezind [7], Majorana and Anile [8], and Ballard and Heavens [9] to name a few.

The interaction between hydrodynamic motion and magnetic field in conducting plasmas are essential in the area of astrophysics, high-energy collision, and geophysics. Two individual cases of magnetohydrodynamic frequented in physics are; the hydrodynamic shock and the electromagnetic wave. As the electromagnetic waves travel at the speed of light, we need to treat the problem relativistically. De Hoffmann and Teller [3] did the same while treating the conducting fluid to be having infinite conductivity. It was achieved by transforming the shock to a frame where the flow velocity is parallel to the magnetic field. This assumption prevents the self-induction of the magnetic field if the fluid is at rest. The infinite conducting fluid assumption is well suited for astrophysical scenarios as the discontinuity interface of the shock is quite small compared to the total radial distance of the star.

The standard technique of writing the jump conditions is to set the divergence of the stress-energy tensor to be zero and use the Gauss's theorem to get the jump conditions across the shock front. The conditions give the general mass, momentum, and energy continuity equations across the front. The three nonmagnetized hydrodynamic equations can be expressed as a single equation known as the Taub adiabat (TA) equation [2,10]. The equation connects the thermodynamic variables of one side of the front with variables on the other side and is deprived of any velocity term. A consistent covariant calculation including the timelike shocks (shocks with a timelike normal vector) was first derived by Csernai [11]. The covariant description also accounts for the shock process including combustion and detonation and their energy release in both spacelike and timelike shocks. In the heavy-ion collision, the hadronization of quark matter can be seen as an example of timelike transition, which has been verified experimentally [12–17].

The astrophysical problem, which frequently deals with hydrodynamic equations, is the phase transition (*PT*) from a neutron star (NS) to a quark star (QS). It was conjectured that at the center of NSs where supranuclear densities are believed to be present, ordinary hadronic matter (HM) is not the stable state of matter [18–20]. At such densities HM is vulnerable to quark matter (QM) (quark being their constituent particles). Therefore, it is likely that a *PT* occurs taking the strongly interacting confined phase (HM) to a deconfined phase (QM). If the QM prevails over a substantial region at the core of an NS, it is referred to as a hybrid star, and if the entire star consists of deconfined quarks, it is known as a strange star.

Such *PT* or conversion in NS is likely to liberate a significant amount of gravitational energy, which can power γ-ray bursts [21,22] and can have gravitational wave signals [23,24]. The initiation of this *PT* can be due to a variety of reasons: starting from cosmological quark nugget [25], mass

*mallick@iiserb.ac.in

accretion [25] to pulsar glitches [26]. The process of *PT* is also widely debated in literature: whether it is detonation or deflagration. One of the most usual ways of studying the *PT* is by employing the hydrodynamic equations. Cho *et al.* [27] were probably the first ones to use the hydrodynamic jump conditions to argue that weak detonation is a possible mode of combustion. However, Tokareva *et al.* [28] and Lugones *et al.* [29] argued that the possible mode of combustion could even be fast detonation. Bhattacharyya *et al.* [30,31] proposed that it can be a detonation or a deflagration depending on the density, whereas Drago *et al.* [32] demonstrated that it is always a deflagration if the process is exothermic. A detailed discussion on such a scenario can be found in a recent paper by Furusawa *et al.* [33].

Most of the studies discussed above employ the relativistic and nonrelativistic RH equations, however, the TA equation is not much studied. The magnetized counterpart of the TA is still to be derived and analyzed. The combustion adiabat (CA) equations are similar to the TA equations only the equation of state (EoS) of, the initial and the final state of matter differs due to the difference of chemical energy. The CA equation is therefore well suited to study the *PT* where the initial state represents the HM, and the final state represents the QM. In this paper, we calculate the magnetized version of the CA equation and employ them to study the astrophysical scenario of *PT*. The usefulness of this equation lies in the fact that they do not involve matter velocities and only deals with the thermodynamic variables of state such as pressure, density, and energy.

The paper is arranged as follows. In Sec. II, we define our problem and the special frame in which we would solve our problem. In Sec. III, we calculate the magnetized TA equations from the conservation equations. Section IV is dedicated to our results, and finally, in Sec. V we summarize our work and draw our conclusions from them.

II. HOFFMANN-TELLER FRAME

For relativistic shocks, the shock jump conditions in the presence of a magnetic field are considerably difficult to solve. The problem becomes more traceable if we write the Rankine-Hugoniot conditions in the de Hoffmann-Teller (HT) frame [3] as done by Ballard and Heavens [9], Kirk and Heavens [34], and Summerlin and Baring [35]. The HT frame is a shock rest frame in which $\vec{v} \times \vec{B} = 0$. This frame can be obtained starting from a local fluid frame by boosting along B [9] or by two successive boosts [35]. We describe both the local fluid frame and HT frame in detail here.

In our actual problem, we have a spherical symmetric neutron star having a poloidal magnetic field, undergoes a phase transition from hadronic matter to quark matter. The shock position at the instant of time is shown in Fig. 1 (blue dot-dashed circle). In this problem, we are assuming a spacelike shock propagating through the medium of NS and converting NS to QS. Let us first assume that the magnetic field is zero in the star. In the local fluid frame, the matter velocities are normal to the shock surface, as shown in Fig. 2(a). Due to the spherical symmetry of our problem, the local fluid frame is also the normal incidence frame (NIF). The quantities in the local fluid NIF frame is represented by primed superscript, whereas the HT frame quantities remain unprimed. For each r and ϕ, we can always represent our system by Fig. 2(a)

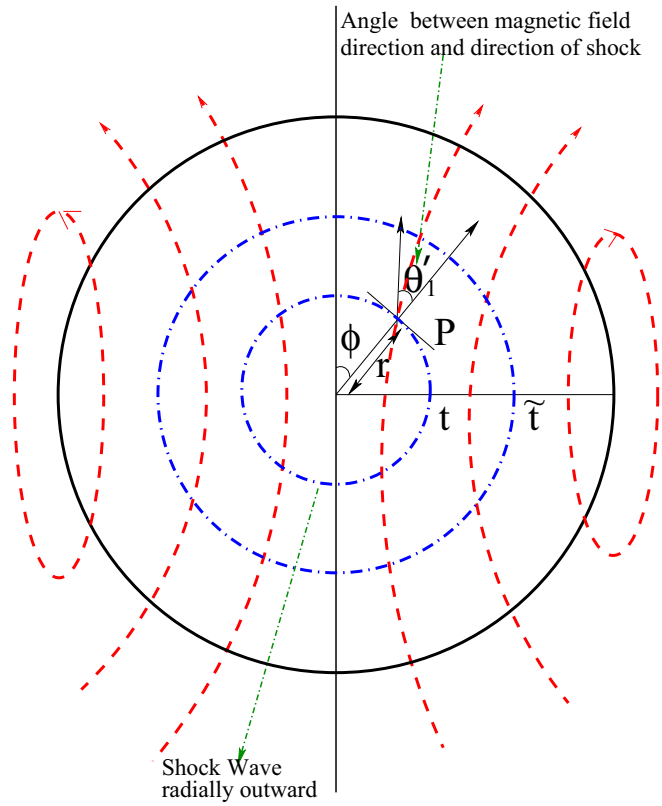

FIG. 1. The evolution of the shock in a magnetized (poloidal field) static star is demonstrated. As the shock grows it moves towards the surface. The shock normal (thin black line) and the magnetic field (red dash curve) are not aligned. The angle between them varies between 0–$\pi/2$ depending on the position of the star. The θ_1' is therefore can vary between 0–$\pi/2$. Here t and $\tilde{t}$ represent the shock front at different instant of time. r is position of shock at time t at a point P and ϕ is latitude of P.

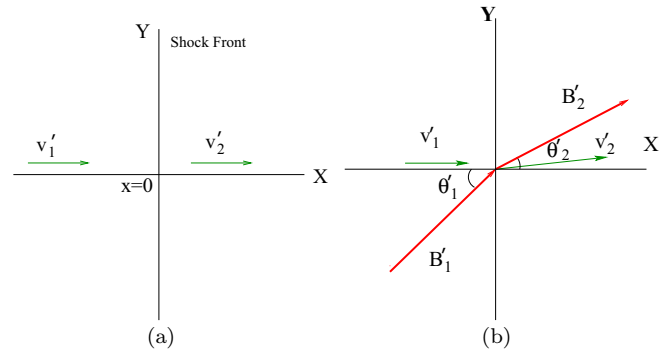

FIG. 2. (a) Illustration of normal shock wave without magnetic field. At $x = 0$ there is shock discontinuity. v_1 and the v_2 are the flow velocities of the upstream and downstream matter, respectively. (b) Shock normal, matter velocities, and the direction of the magnetic field in NIF. Here θ_1' is the angle between the direction of matter flow and the magnetic field B_1' in the upstream matter. The same notations have been followed for the downstream matter.

because our system is spherically symmetric. Now, we go to our actual problem where the star has a poloidal magnetic field. However, the shape of the star is still spherically symmetric. The field is such that it does not produce enough distortion, and the shape of the star remains spherical. For each value of r and ϕ we have different incident angle θ_1' and magnetic filed B_1', as shown in Fig. 2(b). Here, θ_1' is angle between B_1' and upstream matter velocity. The value of θ_1' can vary between 0 to $\frac{\pi}{2}$ depending on the position of the shock.

In the local fluid frame, the upstream matter flows normal to the shock front, but magnetic field makes an angle θ_1', it is called normal incident frame (NIF) [9,34]. The *PT* is brought by a detonation front propagating from the center to surface of the star. In Fig. 1, we show the *PT* in a star. The magnetic field lines are shown by the dashed red line in Fig. 1. The combustion front at the time instant t and a later time $\tilde{t}$ are shown. Point P describes the position of combustion front in the star at a time instant t where front normal makes an angle θ_1' with the magnetic field. As discussed earlier to make the problem solvable, we now move to the HT frame where $\vec{v} \times \vec{B} = 0$ is zero. To get such a frame we will give a Lorentz boost in the y direction ($v_b = v_1' \tan\theta_1'$), where v_b is the boost velocity and $v_1' = v_{1x}'$ is the upstream velocity in the NIF. Such a transformation is restricted by the condition $v_1' \tan\theta_1' < 1$, the condition for subluminal shock [34]. As we would solve our problem in this frame, we represent the variables are unprimed in this frame. In de-HT frame we get,

$$\vec{v} \times \vec{B} = 0 \Rightarrow \frac{B_{1x}}{B_{1y}} = \frac{v_{1x}}{v_{1y}},$$

and we also assume infinite conductivity, which makes the electric field vanish [9,34,35]. Also, the surface current, which appears on the surface between the two phases, is not allowed. The Maxwell condition gives

$$\vec{\nabla} \cdot \vec{B} = 0 \Rightarrow B_{1x} = B_{2x}.$$

The assumptions of infinite conductivity, no surface current, and the alignment of flow velocities and magnetic fields in both upstream and downstream phases result in a particular frame, the HT frame. However, in the HT frame, only subluminal shock can be treated; therefore, we restrict our problem only to spacelike shocks. In this frame TL shock cannot be treated as the assumption does not hold in TL shocks. However, in general, inside a spherically nonrotating star TL combustion can take place. However, the problem needs more general treatment and is much involved. Therefore, to simplify our calculation, we solve this problem in a particular HT frame.

In Fig. 3, we show the space-time diagram of the SL shock. In this figure, we plot the space-time diagram of the *PT* from NM to QM in NS. The combustion front starts at a point near the center of the star and is determined by the Einstein equation, EoS, and some initial discontinuity. The velocity of the collapsing matter is always subluminal, and therefore the shock or the combustion is always SL. The x, y plane is the spatial plane, and the vertical axis is the time t. The configuration of combustion of NM to QM is shown at time t. The star is assumed to be spherically symmetric, and the magnetic field is at an angle to the x axis.

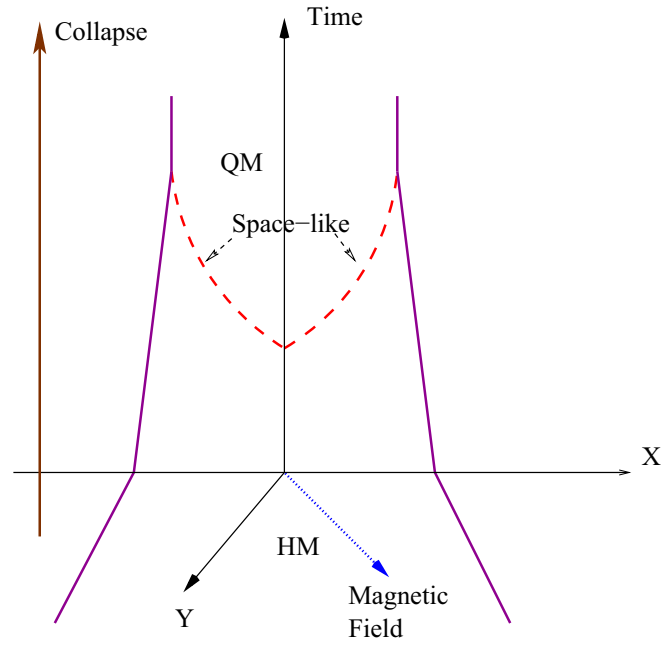

FIG. 3. The space-time diagram of the combustion of NM to QM is illustrated in the figure. Horizontal line is the spatial dimension and the vertical line is the world time t. The configuration of combustion of NM to QM is shown at time t. The star is assumed to be spherically symmetric, and the magnetic field is at an angle to the x axis. The violet (black unbroken) line indicates the surface of the shock a the red (dashed) line indicates the combustion front where the transition of NM to QM happens.

In our calculation we have used a phenomenological magnetic field profile recently formulated by Dexheimer *et al.* [36] where it is described as a function of baryon chemical potential. The magnetic field profile is given by

$$B^*(\mu) = \frac{a + b\mu + c\mu^2}{B_c^2}\mu_M, \tag{1}$$

with coefficients $a = -0.3$, $b = 7.0 \times 10^{-3}$, and $c = -1.0 \times 10^{-7}$. μ is given in MeV and μ_M the dipole magnetic moment in Am^2. The magnetic field is obtained in units of the critical field for the electron, $B_c = 4.414 \times 10^{13}$ G.

In Fig. 1, we show the magnetic profile of the star. The actual magnetic field profile can be obtained by solving the full relativistic Einstein-Maxwell equations. However, the calculation is very complicated, and to simplify our task; we use the magnetic field profile recently formulated by Dexheimer *et al.* [36]. The contribution of the energy-momentum tensor from matter always dominates over the magnetic contribution in a stable star. If the magnetic field strength is less than 10^{17} G near the center of the star, the effect due to the magnetic field becomes negligible. To have a sizable effect, the magnetic field strength has to be in the range 10^{17}–10^{18}G at the interior of the star. In the star, the magnetic field is poloidal along the polar direction, as shown in the figure. In the static star, the shock propagates spherically out of the star. Therefore, the

angle between the shock normal and the magnetic field can vary between 0–$\pi/2$ depending on the shock position (for a particular radial point) with respect to the poloidal field. With the given choice, the maximum magnetic field strength for our calculation (corresponding to the density $n = 1.5$ fm^{-3}) is 1.5×10^{18}G and the minimum (corresponding to the density $n = 0.1$ fm^{-3}) is 4.5×10^{17}G, which is near the surface of the star.

As shown by Dexheimer *et al.*, this field is consistent with the relativistic Einstein-Maxwell equations. It replicates the magnetic field of the star successfully as obtained from solving the full relativistic EM equations. θ_1 determines the contribution of the B_x and B_{1y} in the total magnetic field ($B = \sqrt{B_x^2 + B_{1y}^2}$) for a particular density. As seen from the Fig. 1, θ_1 can vary between 0–$\pi/2$, therefore in our calculation we have taken three values of θ_1. The B_x is kept constant while B_{1y} varies with change in θ_1. When $B_x > B_{1y}$ the angle is small, while when $B_x \simeq B_{1y}$ then the angle is close to 45° and when $B_x < B_{1y}$ the angle exceeds 45°.

We should mention here that the magnetic field can even modify the EoS of the matter. The dependence of the magnetic field on the EoS is evident and telling for a heavy-ion collision, which has been verified by the observation of λ polarization in peripheral collision [37]. The effect of the magnetic field through EoS in gross structure of the NS and its macroscopic properties is not very significant if the field strength is of the order of few times 10^{18} G. It has some effect on the microscopic details, however, to keep our calculation simple, we do not include the magnetic effect on the EoS. This also helps to analyze only the effect of the magnetic field coming from the CA equation.

III. MAGNETIZED TA

We start with a consistent covariant calculation [11,12] to find the equation of the TA in the presence of a magnetic field. Let the discontinuity surface Σ have a normal vector Λ^α. So the normalization condition of this vector given by

$$\Lambda_\alpha \Lambda^\alpha = \begin{cases} +1 & \text{for timelike} \\ -1 & \text{for spacelike.} \end{cases} \tag{2}$$

In the local frame we are taking $\Lambda^\alpha = (1, 0, 0, 0)$ for timelike and $\Lambda^\alpha = (0, 1, 0, 0)$ for spacelike discontinuity. The energy momentum (EM) tensor of this system is given by [38],

$$T^{\alpha\nu} = \omega u^\alpha u^\nu - p g^{\alpha\nu} + T_B^{\alpha\nu}, \tag{3}$$

where, w is the enthalpy ($w = \epsilon + p$), $u^\alpha = (\gamma, \gamma v)$ is the normalized four-velocity of the fluid and γ is the Lorentz factor. $g^{\alpha\nu}$ is metric tensor having sign convention $(+, -, -, -)$; and $T_B^{\alpha\nu}$ is magnetic part of EM tensor, which is given by [39],

$$T_B^{\alpha\nu} = \frac{1}{4\pi}\left(F^{\alpha\lambda}F_\lambda^\nu + \frac{1}{4} g^{\alpha\nu} F^{\lambda\sigma} F_{\lambda\sigma}\right), \tag{4}$$

where $F_{\lambda\sigma}$ is covariant electromagnetic tensor, which is defined as [39]

$$F_{\lambda\sigma} = \partial_\lambda A_\sigma - \partial_\sigma A_\lambda, \tag{5}$$

where $A^\lambda = (\phi, \vec{A})$ is the four-potential (ϕ scalar potential, $\vec{A}$ vector potential). In this paper, we use greek indices to denote space-time coordinate (t, x, y, z).

We define a notation [...] for some quantity C across the discontinuity surface, such as

$$[C] = C_1 - C_2,$$

where subscripts 1 and 2 are used for upstream and downstream matter, respectively. Across the discontinuity surface, the energy, momentum, and number density will remain conserved [11]. The conservation of number density Λ^α is given by

$$[j] = [n^\alpha \Lambda_\alpha] = 0, \tag{6}$$

where $n^\alpha = n u^\alpha$ is the four-current density. The conservation of energy-momentum tensor can be written as

$$[T^{\mu\nu}\Lambda_\nu] = 0. \tag{7}$$

The energy-momentum conservation along the direction of vector Λ^α (normal to the surface of discontinuity Σ), then becomes

$$[T^{\alpha\nu}\Lambda_\alpha\Lambda_\nu] = 0. \tag{8}$$

Using Eq. (3) in above equation we get,

$$\Rightarrow [\omega(u^\alpha\Lambda_\alpha)^2] - [p]\Lambda_\alpha\Lambda^\alpha + \left[T_B^{\alpha\nu}\Lambda_\alpha\Lambda_\nu\right] = 0. \tag{9}$$

Therefore, the square of the current density can be written as

$$j^2 = \frac{[p]\Lambda_\alpha\Lambda^\alpha - \left[T_B^{\alpha\nu}\Lambda_\alpha\Lambda_\nu\right]}{\left[\frac{\omega}{n^2}\right]}, \tag{10}$$

where $T_B^{\alpha\nu}$ is the magnetic part of energy momentum tensor given in Eq. (4).

Now we define a vector G^α normal to Λ_α as (projection of $T^{\mu\nu}\Lambda_\nu$ along the surface Σ)

$$G^\alpha = T_{\tau\sigma}\Lambda^\sigma P^{\alpha\tau}, \tag{11}$$

where

$$P^{\alpha\nu} = g^{\alpha\nu} - \frac{\Lambda^\alpha\Lambda^\nu}{\Lambda_\beta\Lambda^\beta}.$$

Using the Eq. (3) and the definition of $P^{\alpha\nu}$ we get,

$$G^\alpha = \omega(u_\nu\Lambda^\nu)u^\alpha - \frac{\omega(u_\nu\Lambda^\nu)^2\Lambda^\alpha}{\Lambda_\beta\Lambda^\beta} + T_{B\lambda\nu}\Lambda^\nu g^{\alpha\lambda} - \frac{T_{B\lambda\nu}\Lambda^\lambda\Lambda^\nu\Lambda^\alpha}{\Lambda_\beta\Lambda^\beta}. \tag{12}$$

The conservation of energy-momentum tensor normal to the Λ^α is given by

$$G_1^\alpha = G_2^\alpha \Rightarrow [G^\alpha] = 0, \tag{13}$$

which take the form,

$$[\omega(u_\nu\Lambda^\nu)u^\alpha] - \frac{[\omega(u_\nu\Lambda^\nu)^2\Lambda^\alpha]}{\Lambda_\beta\Lambda^\beta} + [T_{B\lambda\nu}\Lambda^\nu g^{\alpha\lambda}] - \frac{[T_{B\lambda\nu}\Lambda^\lambda\Lambda^\nu\Lambda^\alpha]}{\Lambda_\beta\Lambda^\beta} = 0. \tag{14}$$

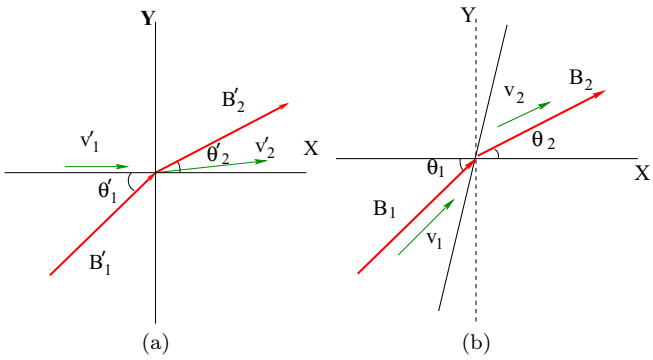

FIG. 4. The shock normal, the matter velocities, and the direction of the magnetic field are shown in the (a) NIF and (b) HT frame. In HT frame the matter velocities and the magnetic field are parallel. The shock is propagating from right to left converting phase 1 to phase 2. θ_1 is the angle that the shock normal makes with the magnetic field (also the same angle with matter velocity) for the upstream phase. θ_2 is the angle subtended in the downstream phase.

Having written down the basic formalism in the covariant form, we now go to a particular frame known as the Hoffmann-Teller (HT) frame [3]. We do not present a general solution to the problem, and we show our results for this particular HT frame. In this frame, the magnetic field and the matter velocities are aligned [3,9,34]. We also assume that the fluid is infinitely conducting, which makes the electric field disappear [3,9]. Also, the surface current, which appears on the surface between the two phases, is not allowed. In Fig. 4, we present the detailed diagram of the shock plane, the velocity, and the magnetic field direction. The continuity equations across the front for a magnetized shock is calculated in detail by Mallick and Schramm [38] and Mallick and Singh [40], and we mention only the details here.

We assume that x direction is normal to the shock plane. The magnetic field is constant and lies in the x-y plane. Therefore the velocities and the magnetic fields are given by v_x and v_y and by B_x and B_y, respectively. The pressure and energy density are denoted by p and ϵ, whereas the baryon density is denoted as n. The angle between the magnetic field and the shock normal in the HT frame is denoted by θ (θ_1 being the incidence angle and θ_2 the reflected angle). We assume that the *PT* happens as a single discontinuity separating the two phases. Therefore we denote 1 as the initial state ahead of the shock (HM or upstream) and 2 as the final state behind the shock (QM or downstream). The shock is propagating from right to left.

The Maxwell equation of no magnetic monopoles(in the covariant form) is given by [39]

$$\partial_\alpha\left(\tfrac{1}{2}\epsilon^{\alpha\beta\gamma\delta}F_{\gamma\delta}\right) = 0, \tag{15}$$

where $\epsilon^{\alpha\beta\gamma\delta}$ is Levi-Civita tensor. In the HT frame the equation becomes $B_{1x} = B_{2x} = B_x$, where B_x is the magnetic field in the x direction, which is same in both the phases. B_{1y} and B_{2y} are magnetic fields in the y direction in phases 1 and 2, respectively. Since our frame is tilted slightly from the y axis, the magnetic field in y direction is not same in two phases.

For the HT frame we have

$$\frac{v_{1y}}{v_{1x}} = \frac{B_{1y}}{B_x} \equiv \tan\theta_1, \tag{16}$$

$$\frac{v_{2y}}{v_{2x}} = \frac{B_{2y}}{B_x} \equiv \tan\theta_2. \tag{17}$$

Therefore, we can write the y component of velocity in terms of x component as

$$v_{1y} = \frac{B_{1y}}{B_x}v_{1x}. \tag{18}$$

In the HT frame we can also write the components of energy momentum tensor for electromagnetic field

$$T_B^{00} = \frac{B_x^2 + B_y^2}{8\pi}, \tag{19}$$

$$T_B^{ik} = \frac{B_x^2 + B_y^2}{8\pi}\delta^{ik} - \frac{B^iB^k}{4\pi}, \tag{20}$$

where B^i (or B^k) is ith (or kth) component of magnetic field vector [i and k denote the spacial (x, y) component of the vector]; and B_x and B_y magnetic field components in x and y direction, respectively.

The four-velocity is defined as

$$u_{1i} = v_{1i}\gamma_1 \Rightarrow u_{1x} = v_{1x}\gamma_1 \quad \text{and} \quad u_{1y} = v_{1y}\gamma_1.$$

The mass flux j in the x direction [from Eq. (6)] is defined as

$$n_1u_{1x} = n_2u_{2x} = j. \tag{21}$$

The four-velocity in then defined as

$$u_{1x} = \frac{j}{n_1} = jV_1 \quad \text{and} \quad u_{2x} = \frac{j}{n_2} = jV_2, \tag{22}$$

where V_a's are the specific volumes (a can represent either one of the phases 1 or 2).

SL discontinuity in HT frame

As the HT frame is only suitable for describing the SL discontinuity, we only analyze the SL shock. The conservation of number density [from Eq. (6)] with $\Lambda^\alpha = (0, 1, 0, 0)$) can be written as

$$n_1\gamma_1v_{1x} = n_2\gamma_2v_{2x}. \tag{23}$$

Implementing Eq. (2) for the spacelike discontinuity, Eq. (9) reduces to

$$\left[\omega\gamma^2v_x^2\right] + [p] + \frac{\left[B_y^2\right]}{8\pi} = 0. \tag{24}$$

The temporal component of Eq. (14) (for spacelike shocks) can be written as

$$[\omega\gamma^2v_x] = 0, \tag{25}$$

and the spacial component as

$$[\omega\gamma^2v_xv_y] - \frac{B_x[B_y]}{4\pi} = 0. \tag{26}$$

Using Eq. (18), Eq. (26) can be rewritten as

$$(B_{1y}\mu_1j^2V_1 - B_{2y}\mu_2j^2V_2) = \frac{B_x^2}{4\pi}(B_{1y} - B_{2y}), \tag{27}$$

which can be further simplified to give

$$B_{2y} = B_{1y}\frac{\mu_1 V_1 j^2 - \frac{B_x^2}{4\pi}}{\mu_2 V_2 j^2 - \frac{B_x^2}{4\pi}} \tag{28}$$

and we can find j^2,

$$j^2 = \frac{B_x^2(B_{1y} - B_{2y})}{4\pi(B_{1y}\mu_1 V_1 - B_{2y}\mu_2 V_2)}. \tag{29}$$

Using the definitions from Eq. (22), Eq. (25) can be redefined as

$$\begin{aligned} \omega_1 u_{1x}\gamma_1 &= \omega_2 u_{2x}\gamma_2 \\ \Rightarrow \omega_1 j V_1 \gamma_1 &= \omega_2 j V_2 \gamma_2 \\ \Rightarrow \omega_1 V_1 \gamma_1 &= \omega_2 V_2 \gamma_2, \end{aligned}$$

which ultimately reduces to

$$\mu_1\gamma_1 = \mu_2\gamma_2. \tag{30}$$

With the definition of modified pressure $\bar{p}_a = p_a + \frac{B_{ay}^2}{8\pi}$, where a can take values 1 and 2 for upstream and the downstream matter, respectively, Eq. (24) reduces to

$$[\omega V^2]j^2 + [\bar{p}] = 0 \tag{31}$$

and the square of the mass flux j^2 becomes

$$\Rightarrow j^2 = -\frac{[\bar{p}]}{[\mu V]}. \tag{32}$$

Using the above definition of j^2 in Eq. (28) we can solve for B_{2y}.

Multiplying Eq. (32) by $(\mu_1 V_1 + \mu_2 V_2)$, and with the definition of $j^2 = \frac{u_{2x}^2}{V_2^2} = \frac{u_{1x}^2}{V_1^2}$ and performing a little algebra, we have the relation

$$\mu_2^2 u_{2x}^2 - \mu_1^2 u_{1x}^2 = (\bar{p}_1 - \bar{p}_2)(\mu_1 V_1 + \mu_2 V_2). \tag{33}$$

Squaring Eq. (30) and then subtracting Eq. (33) from it, we have

$$\mu_2^2\left(u_{2x}^2 - \gamma_2^2\right) - \mu_1^2\left(u_{1x}^2 - \gamma_1^2\right) = (\bar{p}_1 - \bar{p}_2)(\mu_1 V_1 + \mu_2 V_2). \tag{34}$$

With the definition of u_{1x} and γ, and adding and subtracting $\frac{v_{1y}^2}{1 - v_{1x}^2 - v_{1y}^2}$, we have $u_{1x}^2 - \gamma_1^2 = -1 - u_{1y}^2$. The above equation can also be written in terms of magnetic fields

$$u_{1x}^2 - \gamma_1^2 = -1 - \frac{B_{1y}^2}{B_x^2} j^2 V_1^2. \tag{35}$$

Using Eq. (29) and Eq. (35), we can write

$$u_{1x}^2 - \gamma_1^2 = -1 - \frac{B_{1y}^2 V_1^2 (B_{1y} - B_{2y})}{4\pi(B_{1y}\mu_1 V_1 - B_{2y}\mu_2 V_2)}. \tag{36}$$

Similarly we can write

$$u_{2x}^2 - \gamma_2^2 = -1 - \frac{B_{2y}^2 V_2^2 (B_{1y} - B_{2y})}{4\pi(B_{1y}\mu_1 V_1 - B_{2y}\mu_2 V_2)}. \tag{37}$$

Inserting Eq. (36) and Eq. (37) in Eq. (34) and defining,

$$\bar{\mu}_a^2 = \mu_a^2\left[1 + \frac{B_{ay}^2 V_a^2 (B_{1y} - B_{2y})}{4\pi(B_{1y}\mu_1 V_1 - B_{2y}\mu_2 V_2)}\right]$$

$$\boxed{\bar{\mu}_2^2 - \bar{\mu}_1^2 = (\bar{p}_2 - \bar{p}_1)(\mu_1 V_1 + \mu_2 V_2)}. \tag{38}$$

Defining $V_a = \frac{1}{n_a}$ and $X_a = \frac{\omega_a}{n_a^2}$, then the above equation can be rewritten as

$$\boxed{\omega_2 \bar{X}_2 - \omega_1 \bar{X}_1 = (\bar{p}_2 - \bar{p}_1)(X_2 + X_1)}, \tag{39}$$

where $\bar{X}_a = X_a[1 + Y\frac{B_{ay}^2}{n_a^2}]$ and Y is defined as $Y = \frac{B_{1y} - B_{2y}}{4\pi(B_{1y}X_1 - B_{2y}X_2)}$. Here a can take values 1 and 2 for upstream and the downstream matter, respectively.

The above equation is the magnetized Taub adiabat (MTA) equation. The equation is independent of velocity, and only the thermodynamic variables and magnetic field components are present. In the limit $B_{1y} = B_{2y} = 0$ or even for equal magnetic field $B_{1y} = B_{2y} \neq 0$ this reduces to

$$\mu_2^2 - \mu_1^2 = (p_2 - p_1)(\mu_1 V_1 + \mu_2 V_2), \tag{40}$$

the general TA.

The upstream and downstream variables can be used to calculate the matter velocities of both the region. With the notation of m, l, k_1, k_2, d_1, d_2, and s as

$$\begin{aligned} l &= \left(1 + \frac{B_{1y}^2}{B_x^2}\right), \\ m &= \left(1 + \frac{B_{2y}^2}{B_x^2}\right). \\ s &= \sqrt{\omega_1^2 + \omega_2^2 - 2\omega_1\{\omega_2 + 2m(\bar{p}_1 - \bar{p}_2)\} + 4\omega_2 l(\bar{p}_1 - \bar{p}_2) + 4ml(\bar{p}_1 - \bar{p}_2)^2} \\ k_1 &= \omega_1^2 + 2l\{\omega_2 + m(\bar{p}_1 - \bar{p}_2)\}(\bar{p}_1 - \bar{p}_2) - \omega_1\omega_2 - 2m\omega_1(\bar{p}_1 - \bar{p}_2) \\ d_1 &= 2[\omega_1 m - l\{\omega_2 + m(\bar{p}_1 - \bar{p}_2)\}][\omega_1 + l(\bar{p}_2 - \bar{p}_1)] \\ k_2 &= \omega_2^2 - 2m(\bar{p}_1 - \bar{p}_2)\{\omega_1 + l(-\bar{p}_1 + \bar{p}_2)\} - \omega_2\{\omega_1 + 2l(-\bar{p}_1 + \bar{p}_2)\} \\ d_2 &= 2[-\omega_1 m + l\{\omega_2 + m(\bar{p}_1 - \bar{p}_2)\}][\omega_2 + m(\bar{p}_1 - \bar{p}_2)] \end{aligned}$$

the RH equations can be solved for the matter velocities in terms of the thermodynamic variables and magnetic fields. The velocities can be simply written as

$$v_1^2 = \frac{k_1 \pm s\omega_1}{d_1}; \tag{41}$$

$$v_2^2 = \frac{k_2 \pm s\omega_2}{d_2}. \tag{42}$$

In the absence of magnetic field $m = l = 1$ and s reduced to $\sqrt{e_1 - e_2 - p_1 + p_2}$. The two roots of the velocities (v_1^2 and v_2^2) in Eqs. (41) and (42) become the same and reduced to the following form:

$$v_1^2 = \frac{(e_2 + p_1)(p_1 - p_2)}{(e_1 - e_2)(e_1 + p_2)}, \tag{43}$$

$$v_2^2 = \frac{(e_1 + p_2)(p_1 - p_2)}{(e_1 - e_2)(e_2 + p_1)}, \tag{44}$$

which is same as the velocity of the matter phases in the absence of magnetic field. The two solutions (roots) for the velocities are not surprising if we look into the RH equations carefully. The equations are quadratic equations in the velocities (having v_a^2 and v_a term explicitly and also in the γ_a's). Therefore, it is expected that the velocities should have two roots as obtained in this case. However, in the nonmagnetic case, the two roots become equal.

IV. RESULTS

Our results are obtained in the HT frame, and the figures are also drawn in the HT (unprimed) frame. Going from the HT frame to the local frame of the fluid is trivial as the physical variables p, n does not change but the velocity and the angle would change by a constant factor [9,23,34].

As discussed in the earlier section, to solve the MTA equation, we need to know the EoS of both the upstream and downstream phases *a priori*. For the astrophysical calculation related to the *PT* of NS, we assume that the hadronic phase as the upstream phase and quark as the downstream phase. For the hadronic phase, we adopt a relativistic mean-field approach, which is generally used to describe the HM in NSs. In our present calculation, we mostly use PLZ parameter setting [41]; however, for comparisons, we also use NL3 parameter setting [42]. The details of the EoS can be found in many references [24,40,41], and we do not discuss them in detail here.

The QM is described using MIT bag model [43] along with the quark interaction term. The grand potential of the model is given by

$$\Omega_Q = \sum_i \Omega_i + \frac{\mu^4}{108\pi^2}(1 - a_4) + B_g, \tag{45}$$

where i stands for quarks and leptons, Ω_i signifies the potential for species i and B_g is the bag constant with a_4 being the quark interaction parameter, varied between 1 (no interaction) and 0 (full interaction). The second term represents the interaction among quarks. We choose the values of $B_g^{1/4} =$ 140 MeV and $a_4 = 0.55$.

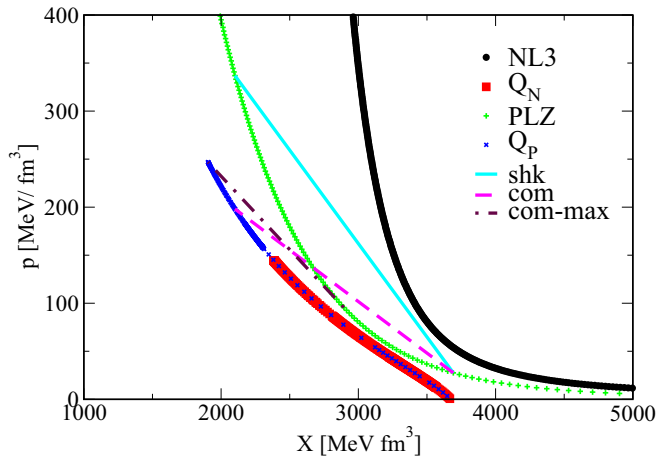

FIG. 5. The TA (p vs. X) curves for HM (NL3 (thick black dotted rightmost curve) and the PLZ (green (light gray marked with plus marks) curve extending to the top) with their corresponding burn state with Q_N and Q_P marked by the square red (dark gray thick short) curve and cross blue (thin black short curve overlying the red curve) curve are drawn. The Q_P curve extends much beyond the corresponding Q_N curve. The upstream point lies on the black/green curve whereas the downstream points lie on the red/blue. The Rayleigh lines (RL) are the straight lines. The RL connecting two points in the same hadronic (PLZ) curve is marked as shk [light blue (gray) line]. This represents a shock or TA. The RL connecting two points of the different curve represent the CA (marked as com and com-max). The com-max [dash-dot brown (almost black) line] is the RL connecting the maximum point of the downstream adiabat with its corresponding point on the upstream curve.

In this calculation we consider a combustion front generated at the center of the star and spreading radially outward in a spherically symmetric star. The combustion front converts HM in the star to QM. Ideally, both spacelike and timelike transition can occur; however, in this calculation, we are only concentrating on the SL transition. We are solving our problem in a particular frame known as the HT frame. In this frame, the magnetic field has a considerable effect on the SL transition; however, the TL transition does not have any magnetic effect. Therefore, we are analyzing the SL CA and its implication in the astrophysical scenario of a neutron star.

For the case of MTA, both the initial and final state belongs to the same EoS (same functions of pressure, energy density, and density) hence lying on a single curve. However, the form of the equation still holds if the initial and final states are from different EoS. As the EoSs of the initial and final state are different the final-state curve shifts from the initial-state curve due to the difference of the chemical energy, there is combustion from the initial state to the final state. The equations [Eqs. (39) and (28)] connecting the initial and final state having different EoS are called the magnetized combustion adiabat (MCA) equations. The curves are called MCA.

The downstream quantities (denoted by subscript 2) are calculated from the known upstream quantities (subscript 1). For a given EoS of HM, we plot a curve in the X, p plane indicated by NL3/PLZ in Fig. 5. The magnetic field at that density is obtained from Eq. (1). Using these as the

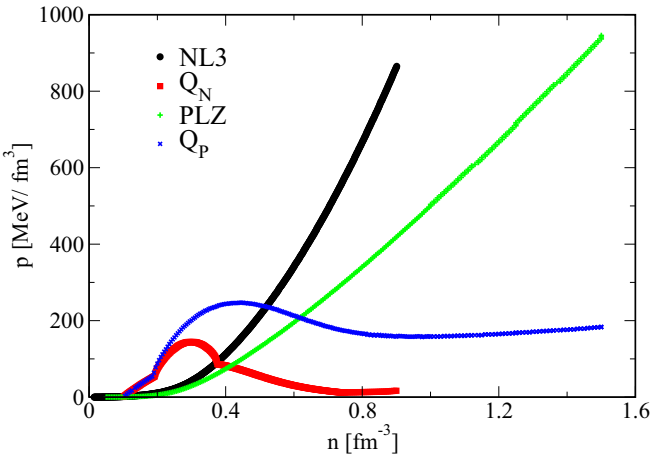

FIG. 6. p as a function of n for HM [NL3 (thick black curve marked with circular dots extending upwards] and the PLZ [green (thin light gray marked with plus) curve] and their corresponding downstream QM (Q_N and Q_P marked by the square red (dark gray thick short) curve and cross blue (thin black curve lying just above the red curve) are illustrated in the figure. The burnt pressure cuts their corresponding HM pressure curves at higher n values.

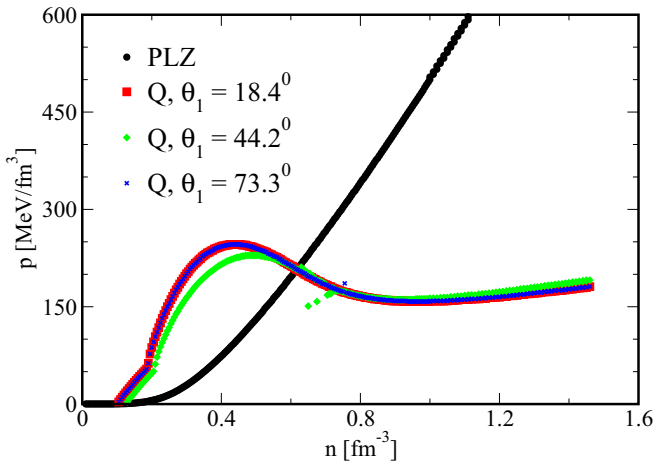

FIG. 7. p as a function of n for PLZ parameter and the burnt pressure of the QM are drawn. The PLZ curve is the thick black curve extending upward. The burnt curves are drawn for three θ_1 values. The curve for 18.4° [thick red (dark gray) curve] and 73.3° [thin blue (almost black) curve] overlaps with each other. The curve with $\theta_1 = 44.2°$ [green (light gray) curve] lies just below these curves initially. The crossing point of the hadronic pressure and quark pressure is the same for all three θ_1 values.

input values for the MCA equations [Eqs. (39) and (28)], we calculate the corresponding QM pressure and magnetic field. From the EoS of QM, the corresponding density and enthalpy are also obtained. Therefore, for a given initial state of the HM, the final burned downstream state will lie on a different curve corresponding to the QM, indicating a burning or in our case a *PT*.

The MCA equations are solved for the downstream quantities treating the upstream quantities as an input. Starting from a point (X_1, p_1) (Fig. 5) in the HM curve if we encounter some point (X_1^*, p_1^*) in the same curve, we have a shock denoted by "shk" in Fig. 5 (shown only for PLZ EoS). However, with the same starting point, if we reach a point (X_2, p_2) having different EoS (in this case Q_P), we will either have a detonation or a deflagration. Gradually changing the input values (X_1, p_1) we generate the upstream curve. Using the points of this curve as input and solving the two equations [Eqs. (28) and (39)] for the QM EoS we generate the downstream curve (X_2, p_2).

In Fig. 6, we show the pressure of the upstream region and the downstream region as a function of baryon density ($n = n_1$). The HM pressure rises monotonically. However, the downstream or QM pressure initially increases and then comes down. It crosses the HM curve at a larger density than two-time nuclear density. We have shown our results for two HM EoSs. This figure is conjugate to Fig. 5. As we proceed upward along the upstream curve (Fig. 5) treating its points as an input to the CA equation, we see that the downstream curve also moves upward. However, after a certain point, although the upstream curve rises, the downstream trajectory does not grow but retraces its path. Hence, there is a maximum point for the downstream pressure. This maximum point of the downstream path coincides with the maximum of the pressure in Fig. 6. The maximum of the pressure is related to the maximum mass of QS and is discussed in great detail in our recent paper [44]. We do not address them further in the present paper.

The x component of the magnetic field does not change in the HT frame, and the only change is in the y component. The variation of the magnetic field along the star is poloidal in nature as described in Eq. (1). With the given configuration, the magnetic field strength at $n = 1.5$ fm^{-3}) is 1.5×10^{18} G while at the lowest density it is 4.5×10^{17} G. This variation of B_x is constant, however, B_{1y} can change with a change in θ_1 [according to Eq. (16)]. When $B_x > B_{1y}$ the angle is small, while when $B_x \simeq B_{1y}$ then the angle is close to 45° and when $B_x < B_{1y}$ the angle exceeds 45°.

In Fig. 7 we plot the pressure as a function of density for three different θ_1 values. For the two extreme cases, ($\theta_1 \neq 44.2°$) the nature of the pressure curves are quite similar. However, for $\theta_1 = 44.2°$, the downstream pressure is always less than the other two, though the crossing of the hadronic and quark pressures coincides. Beyond that, all the curves almost overlap. We plot the CA curves in Fig. 8. The retracing of the quark trajectory can still be seen in all the curves, however, for the curve with $\theta_1 = 44.2°$ it occurs from a lesser pressure value.

A change in the upstream angle imparts a change in the downstream angle as illustrated in Fig. 9. For small θ_1, the downstream θ_2 first rises with an increase in density and reaches a maximum angle of 21° and then decreases gradually with density finally coinciding with θ_1. At further large densities θ_2 becomes slightly smaller than θ_1. For $\theta_1 = 44.2°$ the initial rise in θ_2 is much sharper and attains a maximum value of 49° after which it gradually decreases. The nature of the curve is similar to that of the previous case. However, for large angles, θ_2 is almost equal to θ_1 and both the curves overlap.

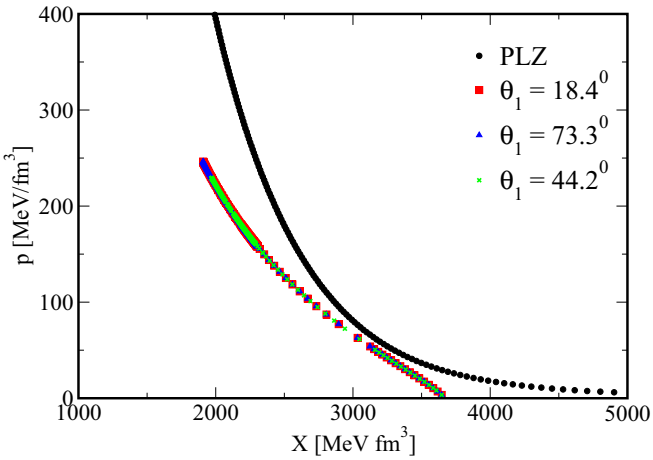

FIG. 8. The CA (p vs. X) curves for PLZ parameter (thick black curve extending to the top) and the burnt pressure of the QM is drawn. The curves are drawn for three angular values between the shock front and matter velocity. All the burnt curves overlap with each other. The burnt curve for $\theta_1 = 44.2^\circ$ [green (light gray) shortest curve] retraces from lower point than the other two curves. Here curve for $\theta_1 = 73.3^\circ$ is plotted before $\theta_1 = 44.2^\circ$ curve to emphasize that the latter curve maximum pressure value is lower than former curve.

The nature of θ_1 and θ_2 is very important in determining B_{2y}. In Fig. 10 we plot the ratio of B_{2y} to B_{1y} against baryon number density. For the case $\theta_1 = 18.4^\circ$, at low densities B_{2y} is greater than B_{1y} and the ratio B_{2y}/B_{1y} increases with density, reaching a maximum at around $n = 0.3$ fm^{-3}. The ratio becomes 1 at $n = 0.64$ fm^{-3} and continues to be so for some density range. Beyond $n = 0.73$ fm^{-3}, B_{2y} then becomes smaller than B_{1y}. For $\theta_1 = 44.2^\circ$, at low densities B_{2y} is much larger than B_{1y} and increases further with density. The nature

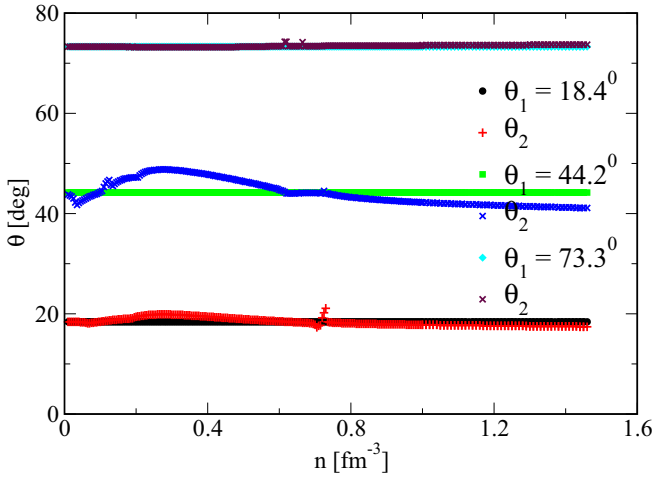

FIG. 9. The angle between downstream velocity and the shock perpendicular is shown for three different input angles (θ_1). The input angle for a particular analysis is constant [three straight lines, lower black, middle green (gray) and the top light blue (gray)] whereas the output angle θ_2 [nonlinear curves, lower red (dark gray), middle blue (almost black) and the top brown (dark gray) curves] varies with density.

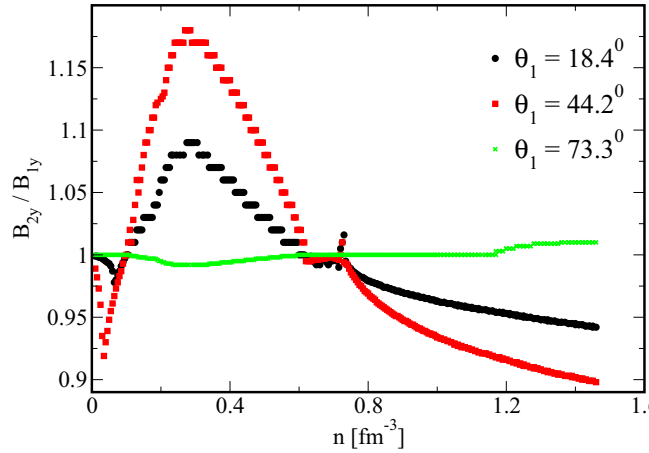

FIG. 10. The ratio of B_{2y}/B_{1y} as a function of n is shown. The ratio is shown for three input θ_1 values, where value 1 of the y axis indicates $B_{2y} = B_{1y}$.

of the curve is similar to that of $\theta_1 = 18.4^\circ$ only differing quantitatively. For $\theta_1 = 73.3^\circ$, the nature is quite different and B_{2y} is almost equal to B_{1y} throughout the density range. The change in the y component of the magnetic field is responsible for the change in the total magnetic field of the QS concerning that of the magnetic field of an NS. The total magnetic field is given by

$$B_a = \sqrt{B_x^2 + B_{ay}^2}. \tag{46}$$

Solving the conservation conditions, we can find the matter velocities of the upstream and downstream region in terms of the thermodynamic variables and the magnetic field as derived in Eqs. (41) and (42). In Fig. 11 we have plotted the velocity as a function of density. Here both the roots of Eqs. (41) and (42) contribute to the matter velocities. For the first case, ($\theta_1 = 18.4^\circ$) both v_1 and v_2 initially increase with density, but v_1 is always greater than v_2. v_1 rises much faster and reaches a peak at $n = 0.24$ fm^{-3} beyond which it decreases becoming zero at $n = 0.74$ fm^{-3}. v_2 also increases with density (not as steeply as v_1) and then becomes flatter beyond $n = 0.25$ fm^{-3}. The plateau region continues until $n = 0.64$ fm^{-3} beyond which it falls steeply to zero. The velocities now become either zero or are unphysical. At much higher densities v_1 and v_2 again becomes finite. However, at such high densities, initially, the velocity is close to 1 and decreases with an increase in density. In this regime, v_2 is always greater than v_1 implying a slow combustion process. For $\theta = 44.2^\circ$, both v_1 and v_2 are similar to the previous curves, only differing quantitatively.

The nature of the curve for $\theta_1 = 73.3^\circ$ is quite different. At low density v_1 increases with density and reaches a maximum at $n \simeq 0.15$ fm^{-3}, and then gradually decreasing to becomes zero at $n = 0.6$ fm^{-3}. Beyond $n = 0.7$ fm^{-3} v_1 takes a constant value of 0.29. The v_2 curve is totally an inverse of the v_1 curve. Initially it decreases with density from value 1 forming a U-shaped curve between $n = 0.14$ fm^{-3} and $n = 0.53$ fm^{-3}. Beyond that it also assumes a constant value of 0.29. In this case v_2 is always greater than v_1 implying a fast detonation.

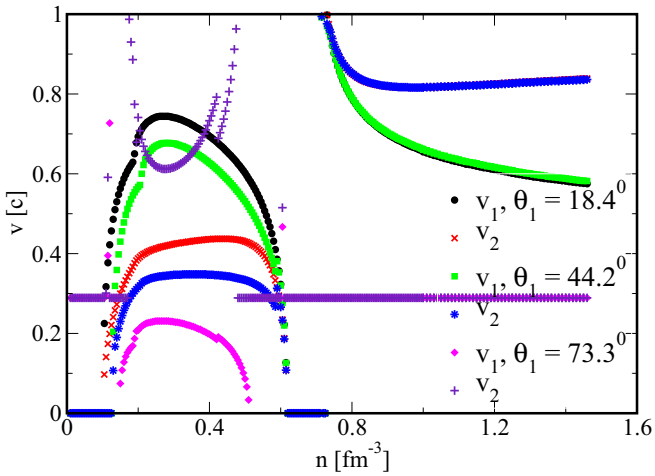

FIG. 11. The upstream (v_1) and downstream (v_2) velocities are shown as a function of n. Both v_1 and v_2 first increase till a point, then decrease and go to zero. v_1 is always greater than v_2, however, they reach the maximum point and goes to zero at same n values. The velocities attain large non zero values at much higher densities. v_1's are marked with black dots, square green (light gray) dots and diamond pink (lowest darkish gray) dots. v_2's are marked with cross red (dark gray) marks, star blue (almost black) marks and plus violet (dark gray) marks.

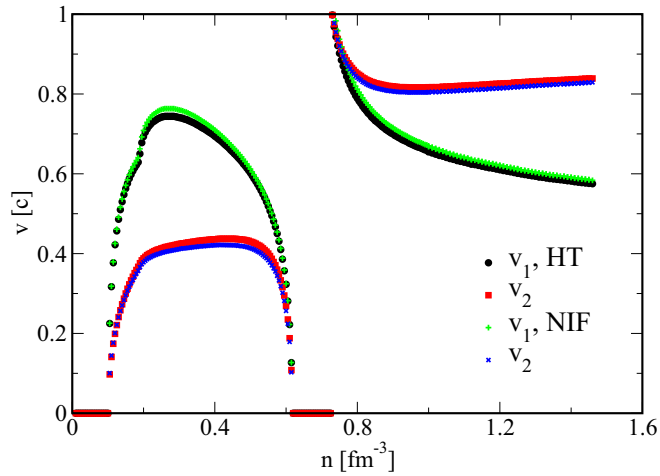

FIG. 12. The upstream and downstream velocities are shown as a function of density for both the HT and the NIF local fluid frame. The HT frame curves are marked with black circular dots (v_1) and square red (gray) dots (v_2). The NI frame curves are marked with plus green (light gray) marks and cross blue (almost black) marks. The results is shown for $\theta_1 = 18.4^\circ$.

The results shown here are for the HT frame. However, our local fluid frame is NIF. Therefore, it is reasonable to recast our results in the NIF. However, in the thermodynamic variables are not frame dependent [9,23,34]. Therefore there is no change in those results. We only need to transform the velocities, the angle, and the x component of the magnetic field when going from HT to the NIF frame. The transformation equation for the velocities are [34,35]

$$v'_{1x} = v_{1x}\Gamma_b \tag{47}$$

$$v'_{1y} = 0 \tag{48}$$

$$v'_{2x} = \Gamma_b \frac{v_{2x} - v_b^2 v_{2x}}{1 - \Gamma_b v_b v_{2y}} \tag{49}$$

$$v'_{2y} = \frac{v'_{2x} v_{2y} - v_{2x} v_b}{v_2 x}, \tag{50}$$

where the boost velocity becomes $v_b = v_{1y}$ and $\Gamma_b = \frac{1}{\sqrt{1-v_b^2}}$. The transformation of the incident and the reflected angle are given by

$$\tan\theta'_1 = \frac{\tan\theta_1}{\Gamma_b} \tag{51}$$

$$\tan\theta'_2 = \frac{\tan\theta_2}{\Gamma_b}. \tag{52}$$

We see that although the angles are frame dependent, the ratios of them are not. Finally, the transformation equation for the magnetic field are given by

$$B'_{ax} = B_{ax}\Gamma_b \tag{53}$$

$$B'_{ay} = B_{ay}, \tag{54}$$

where a can take values either 1 or 2. The y component of the magnetic field does not suffer any change and only the x component of the field changes, however, the ratios are still invariant. Therefore, there is no change in Fig. 10. The final HS magnetic field also does not change considerably.

In Fig. 12 we plot the velocities of the HT frame and NIF frame for $\theta_1 = 18.4^\circ$. The change in the velocities are very nominal, and also the form of the curve remains the same. The change of the velocities for the other two different values of theta is also similar. Finally in Fig. 13 we plot the upstream and downstream angles in the HT and NIF frame. The change in the incident angle is negligible, and we can safely assume that the incident angle in our local fluid frame is also close to $\theta_1 = 18.4^\circ$ and is almost constant. There is a minimal change

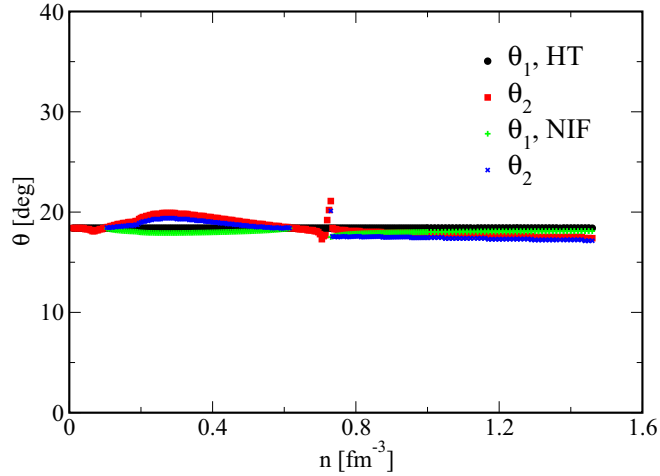

FIG. 13. The incident upstream and the downstream angles are shown as a function of n for both the HT and NIF frame. The nomenclature of the curve remains similar as that of the previous curve. The results is shown for $\theta_1 = 18.4^\circ$.

in the downstream angle (by a maximum of half a degree) but the nature of the curve remains the same. The nature of the curve remains similar to the other two angles as well.

Therefore, we can safely assume that in a star, the incident angle is the same for HT and NIF. Therefore, diagram 1 still remains valid. Going from the HT to NIF the frame, which is the local fluid frame, our conclusion does not change, and there is negligible quantitative change while the qualitatively our results remain the same. Although we have solved in the particular HT frame, our results remain valid even for the local fluid frame. For our spherically symmetric star, our local fluid frame is also the NIF frame. Therefore, we only have to give one boost to go to the HT frame and solve our problem. However, in an axisymmetric star, the local fluid frame may not be the NIF frame and we may need two boosts to go to the HT frame. However, for our calculation in spherically symmetric star, the initial NIF frame is entirely satisfactory.

V. SUMMARY AND CONCLUSION

In this paper, we have derived the MTA/MCA equation in the HT frame, which was never realized before. The HT frame applies only to the SL shocks, and in this frame, the problem becomes relatively manageable. This equation is different from the general conservation equations since the velocity terms are absent. The matter velocities can be calculated from the thermodynamic variables and magnetic fields.

QM CA shows a retracing nature even in magnetized plasmas. The pressure curve obtained from solving the MCA equations has a peak, which is evident from the retracing nature of the CA of QM. The retracing nature of the CA and the maximum value of pressure of QM indicates a mass bound to the QSs assumed to be formed by first-order *PT* [44].

The angle between the matter velocities and the shock front along with the density of the NS is critical in determining the magnetic field of the burnt star and the downstream shock velocity angle. This can have a significant observational consequence as it could determine whether the *PT* to a QS would result in a star, less or more magnetic than the initial NS. The initial tilt angle (angle between the rotational axis and the magnetic axis) is also the angle between the shock front and matter velocity, assuming that the shock spreads spherically in the star. The final tilt of the QS can be different from the initial inclination of the NS. For instance, if an NS of about 1.2–1.4 solar mass with small tilt angle suffers a *PT* the magnetic field of the QS would be larger than the initial NS. However, if the tilt angle is large, the QS has similar field strength as that of the NS. The situation is different for a more massive star, where a *PT* with a small tilt angle would result in a QS whose magnetic field is less than the NS.

The burning mechanism of the star is dependent on the magnetic field, the tilt angle, and the density of the NS. A star of about 1.2–1.5 solar mass with a moderate tilt angle is likely to undergo a detonation ($v_1 > v_2$); however, a massive star of about 1.8–2 solar mass with a small tilt angle is expected to experience a *PT* via a deflagration process. There are some stars that are not prone to *PT* as the velocities become zero for such *PT*. On the other hand, a small-sized star with high tilt angle is likely to undergo a *PT* via deflagration mechanism.

The mass limit of the combusted star depends mostly on the matter properties of the CA equation, whereas the magnetic field and the tilt angle of the combusted star depend on the magnetic field properties of the CA. The change in the magnetic field and the tilt angle can have a significant effect on the observation and detection of an NS or a QS. We should mention that the results are obtained for the particular HT frame where magnetic and flow velocities are parallel both in the upstream and downstream. Also, the surface current is not allowed to appear in the transition surface between HM and QM. The HT restricts the problem to be solvable only for the spacelike shock. However, in general, inside a spherically symmetric nonrotating star, TL combustion can take place. The magnetic field, in general, can also affect the TL combustion (not in HT frame), but a general covariant calculation is complicated. Therefore, to simplify our calculation, we assume a particular HT frame. The general solution to this problem can be interesting and we are in the process trying to address the problem.

Finally, we have transformed our results from the HT frame to the NIF frame, which is also the local fluid frame for a spherically symmetric star. We find that our results do not change much, going from the HT to the local fluid frame. We should mention here that for a nonspherical star, the local fluid frame may not be the NIF frame, and we need two boosts to go into the HT frame. This may bring some quantitative change in the results, but the qualitative nature is expected to remain the same as only the velocities and the incident and reflected angle change going from local to HT frame. However, we are in the process of solving our problem in an axisymmetric star.

To summarize, the MCA equations can be a tool to study *PT* in magnetized NSs. The mechanism and the equations are valid for any hydrodynamic system and can be well suited for earth-based relativistic heavy-ion collision. We are in the process of further analyzing this mechanism and studying other general features of the MCA.

ACKNOWLEDGMENTS

R.M. is grateful to the SERB, Govt. of India for monetary support in the form of Ramanujan Fellowship (SB/S2/RJN-061/2015) and Early Career Research Award (ECR/2016/000161). R.M. and S.S. would also like to thank IISER Bhopal for providing all the research and infrastructure facilities.

[1] L. D. Landau and E. M. Lifshitz, *Fluid Mechanics* (Pergamon Press, Oxford, 1987).
[2] A. H. Taub, Phys. Rev. **74**, 328 (1948).
[3] F. de Hoffmann and E. Teller, Phys. Rev. **80**, 692 (1950).
[4] H. Cabannes, *Theoretical Magnetofluiddynamics* (Academic, New York, 1970).
[5] A. Lichnerowicz, *Relativistic Hydrodynamics and Magnetohydrodynamics* (Benjamin, New York, 1967)

[6] G. M. Webb, G. P. Zank, and J. F. McKenzie, J. Plasma Phys. **37**, 117 (1987).
[7] S. Appl and M. Camenzind, Astron. Astrophys. **206**, 258 (1988).
[8] A. A. Majorana and A. M. Anile, Phys. Fluid **30**, 3045 (1987).
[9] K. R. Ballard and A. F. Heavens, Mon. Not. R. astro. Soc. **251**, 438 (1991).
[10] K. S. Thorne, AstroPhys. J. **179**, 897 (1973).
[11] L. P. Csernai, Zh. Eksp. Teor. Fiz. **92**, 379 (1987) [Sov. JETP **65**, 216 (1987)].
[12] L. P. Csernai, *Introduction to Relativistic Heavy Ion Collisions* (Wiley, Chichester, 1994)
[13] U. W. Heinz and P. F. Kolb, Phys. Lett. B **542**, 216 (2002).
[14] E. Frodermann, R. Chatterjee, and U. Heinz, J. Phys. G **34**, 2249 (2007).
[15] L. P. Csernai, Y. Cheng, S. Horvat, V. Magas, D. Strottman, and M. Zetenyi, J. Phys. G **36**, 064032 (2009).
[16] N. Armesto, A. Dainese, D. d'Enterria, S. Masciocchi, C. Roland, C. A. Salgado, van A. Leeuwen, and U. A. Wiedemann, Nucl. Phys. A **931**, 1163 (2014).
[17] S. Floerchinger and U. A. Wiedemann, Phys. Rev. C **89**, 034914 (2014).
[18] N. Itoh, Prog. Theor. Phys. **44**, 291 (1970).
[19] A. R. Bodmer, Phys. Rev. D **4**, 1601 (1971).
[20] E. Witten, Phys. Rev. D **30**, 272 (1984).
[21] Z. Berezhiani, I. Bombaci, A. Drago, F. Frontera, and A. Lavagno, AstroPhys. J. **586**, 1250 (2003).
[22] R. Mallick and P. K. Sahu, Nucl. Phys. A **921**, 96 (2014).
[23] R. Mallick and S. Schramm, Phys. Rev. C **89**, 045805 (2014).
[24] R. Prasad and R. Mallick, AstroPhys. J. **859**, 57 (2018).
[25] C. Alcock, E. Farhi, and A. Olinto, AstroPhys. J. **310**, 261 (1986).
[26] E. Chubarian, H. Grigorian, S. Poghosyan, and D. Blaschke, Astron. Astrophys. **357**, 968 (2000).
[27] H. T. Cho, K. W. Ng, and A. D. Speliotopoulos, Phys. Lett. B **326**, 111 (1994).
[28] I. Tokareva, A. Nusser, V. Gurovich, and V. Folomeev, Int. J. Mod. Phys. D **14**, 33 (2005).
[29] G. Lugones, O. G. Benvenuto, and H. Vucetich, Phys. Rev. D **50**, 6100 (1994).
[30] A. Bhattacharyya, S. K. Ghosh, P. S. Joarder, R. Mallick, and S. Raha, Phys. Rev. C **74**, 065804 (2006).
[31] I. Mishustin, R. Mallick, R. Nandi, and L. Satarov, Phys. Rev. C **91**, 055806 (2015).
[32] A. Drago, A. Lavagno, and I. Parenti, Astrophys. J. **659**, 1519 (2007).
[33] S. Furusawa, T. Sanada, and S. Yamada, Phys. Rev. D **93**, 043018 (2016).
[34] J. G. Kirk and A. F. Heavens, Mon. Not. R. astro. Soc. **239**, 995 (1989).
[35] E. J. Summerlin and M. G. Baring, Astro Phys. J. **745**, 63 (2012).
[36] V. Dexheimer, B. Franzon, R. O. Gomes, R. L. S. Farias, S. S. Avancini, and S. Schramm, Phys. Lett. B **773**, 487 (2017).
[37] Y. L. Xie, M. Bleicher, H. Stocker, and D. J. Wang, and L. P. Csernai, Phys. Rev. C **94**, 054907 (2016).
[38] R. Mallick and S. Schramm, Phys. Rev. C **89**, 025801 (2014).
[39] J. D. Jackson, *Classical Electrodynamics* (John Wiley, New York 1975).
[40] R. Mallick and A. Singh, Int. J. Mod. Phys. E **27**, 1850083 (2018).
[41] P. G. Reinhard, Z. Phys. A **329**, 257 (1988).
[42] N. K. Glendenning and S. A. Moszkowski, Phys. Rev. Lett. **67**, 2414 (1991).
[43] A. Chodos, R. L. Jaffe, K. Johnson, C. B. Thorn, and V. F. Weisskopf, Phys. Rev. D **9**, 3471 (1974).
[44] R. Mallick and I. Mohammad, Mon. Not. R. astro. Soc. **485**, 577 (2019).